We are IntechOpen, the world's leading publisher of Open Access books Built by scientists, for scientists

4,800
Open access books available

122,000
International authors and editors

135M
Downloads

Our authors are among the

154
Countries delivered to

TOP 1%
most cited scientists

12.2%
Contributors from top 500 universities

CLARIVATE ANALYTICS BOOK CITATION INDEX INDEXED

WEB OF SCIENCE™

Selection of our books indexed in the Book Citation Index in Web of Science™ Core Collection (BKCI)

Interested in publishing with us?
Contact book.department@intechopen.com

Numbers displayed above are based on latest data collected.
For more information visit www.intechopen.com

Chapter 16

A Parallel between Laser Irradiation and Relativistic Electrons Irradiation of Solids

Mihai Oane, Rareş Victor Medianu and Anca Bucă

Additional information is available at the end of the chapter

http://dx.doi.org/10.5772/62353

Abstract

The investigation of the thermal field distribution in a material sample irradiated by a laser beam or an electron beam with the energy of a few MeV appears as a demand for all kinds of experiments that involve irradiation. When investigating the effects of accelerated electrons on a target, it is necessary to figure out the temperature rise in the target. Also during irradiation with laser beams, it is important to know the thermal behavior of the target. A parallel between laser and electron beam irradiation is also made. The results are very interesting. Also, a very interesting case of cluster nano-particles (20–100 nm; inserted in a Cu surface) heated with a laser beam is tacking in to account.

The present chapter is a review article type which comprises the expertise gathers around this domain during the past 15 years within the institute: NILPRP-Romania.

Keywords: laser, electron (beam), irradiation, nano-particle, interaction, W and C

1. Introduction

There are many methods for evaluating the thermal fields in radiation-matter interaction, but most of them require a complex mathematical handling [1–4]. This chapter presents a direct and powerful mathematical approach to compute the thermal field for electron beam-material and laser-sample interaction. The solving procedure is based on applying the integral transform technique which was developed in the 1960s, by the Russian School of Theoretical Physics [5]. As an example, the integral transform technique is used in [3] to solve the heat equation for a sample exposed to an infrared laser beam in order to find the solution for the absorption coefficient, which is then checked experimentally. It should be pointed out straightforwardly

that the heat equation has the same form in the case of irradiation with a laser beam or an electron beam, at sufficiently large beam intensities [6, 7]. There is, however, a disadvantage in this model as it cannot take into account simultaneously the variation with temperature of several thermal parameters involved in the interaction like, for example, the thermal conductivity or thermal diffusivity. In consequence, the model should be regarded as a first approximation of the thermal field. The main advantage is that the solution is a series which converges rapidly. It is important to note that the integral transform technique, as it will be shown in the next sections, belongs to the "family" of Eigen functions and Eigen values-based methods.

2. The applicability of the Fourier heat equation for study of laser-nano particles clusters interaction

Light has always played a central role in the study of physics, chemistry and biology. In the past century, a new form of light, laser light, has provided important contributions to medicine, industrial material processing, data storage, printing and defense [8] applications. In all these areas of applications, the laser-solid interaction played a crucial role. The theory of heat conduction was naturally applied to explain this interaction since it was well studied for a long time [9]. For describing this interaction, the classical heat equation was used in a lot of applications. Apart of some criticism [10], the heat equation still remains one of the most powerful tools in describing most thermal effects in laser-solid interactions [11]. In particular, the heat equation can be used for describing both of light interaction with homogeneous and inhomogeneous solids. In the literature, thus a special attention was given to cases of light interaction with multi-layered samples and thin films.

It is undertaken in the following treatment that it has a solid consisting of a layer of a metal such as Au, Ag, Al or Cu, respectively. Assuming that only a photo-thermal interaction takes place, and that all the absorbed energy is transformed into heat, the linear heat flow in the solid is fully described by the heat partial differential equation, Eq. (1):

$$\frac{\partial^2 T}{\partial x^2}+\frac{\partial^2 T}{\partial y^2}+\frac{\partial^2 T}{\partial z^2}-\frac{1}{\gamma}\frac{\partial T}{\partial t}=-\frac{A(x,y,z,t)}{k} \tag{1}$$

where: T(x, y, z ,t) is the spatial-temporal temperature function, γ is the thermal diffusivity, k is the thermal conductivity and A is the volume heat source (per unit time). In general, one can consider the linear heat transfer approximation and using the integral transform method assume the following form for the solution of the above heat equation, Eq. (2):

$$\begin{aligned} T(x,y,z,t)=&\sum_{i=1}^{\infty}\sum_{j=1}^{\infty}\sum_{k=1}^{\infty} f(\mu_i,\nu_j,\lambda_k)\cdot g(\mu_i,\nu_j,\lambda_k,t)\\ &\times K_x(\mu_i,x)\cdot K_y(\nu_j,y)\cdot K_z(\lambda_k,z) \end{aligned} \tag{2}$$

http://dx.doi.org/10.5772/62353

where: $f(\mu_i, \nu_j, \lambda_k) = \frac{1}{k \cdot C_i \cdot C_j \cdot C_k} \iiint_{0-b-c}^{a\,b\,c} A(x, y, z, t) K_x(\mu_i, x) \cdot K_y(\nu_j, y) \cdot K_z(\lambda_k, z) dxdydz$ and

$$g(\mu_i, \nu_j, \lambda_k, t) = 1/(\mu_i^2 + \nu_j^2 + \lambda_k^2)[1 - e^{-\beta_{ijk}^2 t} - (1 - e^{-\beta_{ijk}^2 (t - t_0)}) \cdot h(t - t_0)] \quad (3)$$

with $\beta_{ijk}^2 = \gamma(\mu_i^2 + \nu_j^2 + \lambda_k^2)$.

Here, t_0 is the light pulse length (assumed rectangular) and h is the step function. The functions $K_x(\mu_i, x)$, $K_y(\nu_j, y)$ and $K_z(\lambda_k, z)$ are the Eigen functions of the integral operators of the heat equation and μ_i, ν_j, λ_k are the Eigen values corresponding to the same operators. Here, for example: $K_x(\mu_i, x) = \cos(\mu_i \cdot x) + (h_{lin}/k \cdot \mu_i) \cdot \sin(\mu_i \cdot x)$, with h_{lin}—the linear heat transfer coefficient of the solid sample along x direction.

The coefficients C_i, C_j and C_k are the normalizing coefficients where, for example: $C_i = \int_{-b}^{b} K_x^2(\mu_i, x) dx$. ($a$, $2b$ and $2c$ are the geometrical target dimensions, which are supposed to be a parallelepiped one).

It has used the thermal parameters of the Cu sample as given in Table 1.

	K [W/cmK]	γ [cm²/s]	α [cm⁻¹]
Cu	3.95	1.14	$7.7 \cdot 10^5$

Table 1. Thermal parameters of Cu.

It has used the heat equation for a configuration where the layers are assumed to have a thickness of 1 mm onto which are included clusters of nano-spheres. The heat term for such a system can be represented by the following equation:

$$A(x, y, z, t) = \sum_{m,n,p} I(x, y, z)((\alpha_1 + r_S \delta(z) + \alpha_{mnp}(\delta(x_m) \cdot \delta(y_n) \cdot \delta(z_p))) \cdot (h(t) - h(t - t_0)) \quad (4)$$

where, m,n,p denote the positions of the nano-particles-clusters, α_1—the optical absorption coefficient, I the incident plane wave radiation intensity incoming from the top –z direction, r_S—the surface absorption coefficient, α_{mnp}—the nano-particles optical absorption coefficients, x,y,t represent the space and time coordinates on the layer surface and h is the step time function.

For the simulation, we have to consider:

$$\alpha_{mnp} >> \alpha_1 + r_S d(z) \tag{5}$$

Inserting groups or clusters of nano-particles-clusters on top of a layer exposed to irradiation gives a detectable increase of temperature in comparison with the bulk material in pure form. This result can be seen in the following simulations.

For m, n = 1, 2 and p = 1, we have plotted in **Figures 1–3**, the thermal field of 1, 2 and 4 nano-particles-clusters for the case of a Cu layer.

The present chapter continues the numerous ideas developed in the past few years with the integral transform technique applied to classical Fourier heat equation [1, 2].

From practical point of view, consider the formula (2), that: i varies from 1 to 100; j varies from 1 to 100, and k varies from 1 to 100. In consequence, the solutions will be like a sum of 1 million functions. In this way, these solutions become from semi-analytical into analytical one. The solutions are easy to compute in MATHEMATICA, or other package software.

In conclusion, it is considered that the method of integral transform technique is a serious candidate in competition with: Born approximation, Green function method or numerical methods. In **Figure 44** is represented the "geometrical" situation for **Figure 3**.

The nano-particles-clusters should be of the order of magnitude of 20 nm, which is the limit of availability of Fourier model [12].

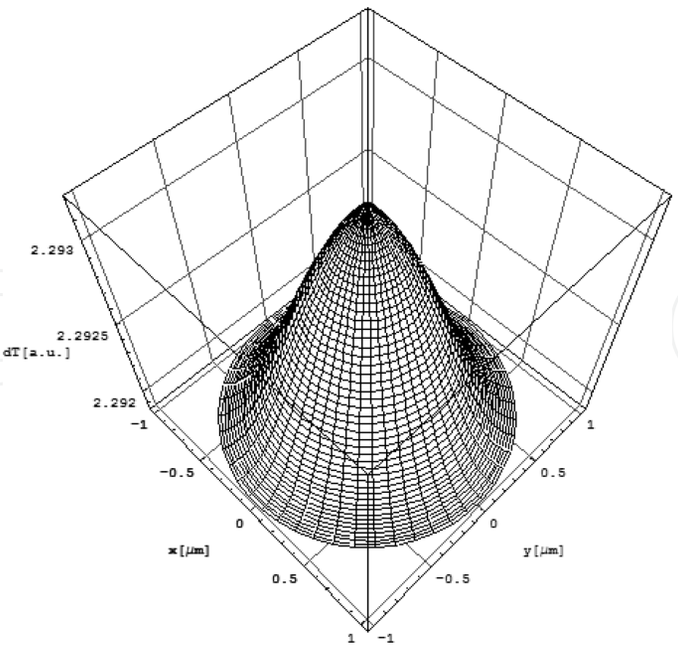

Figure 1. The thermal field produced by one nano-particle-cluster on a Cu substrate. The nano-particle is situated at x = 0 and y = 0, and 200 nm depth inside Cu sample.

http://dx.doi.org/10.5772/62353

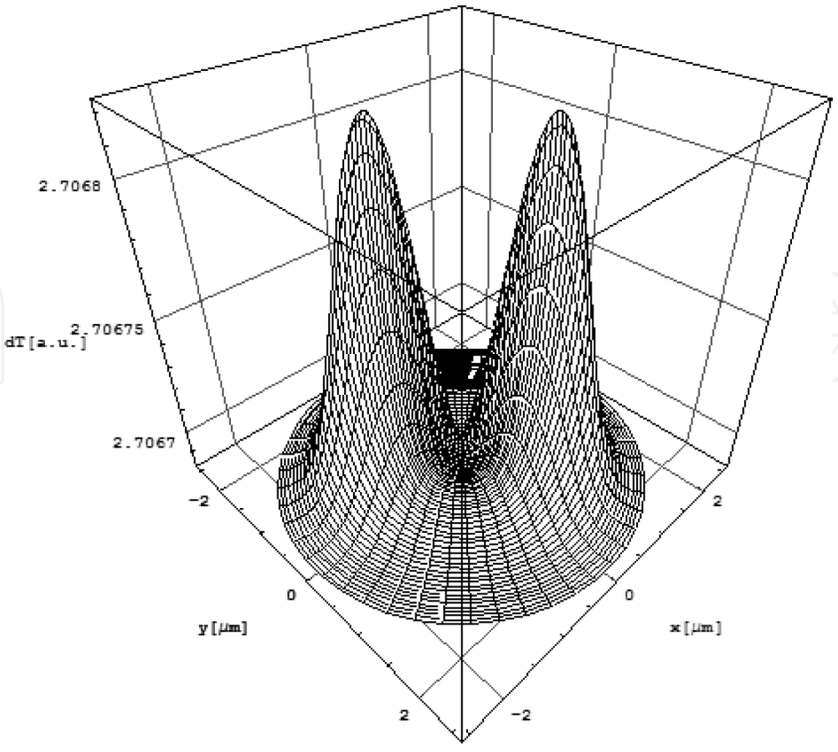

Figure 2. The thermal field produced by two nano-particles-clusters on a Cu substrate. The two nano-particles-clusters have the coordinates symmetric in rapport with the heat source. The two nano-particle-clusters are also 200 nm inside Cu sample.

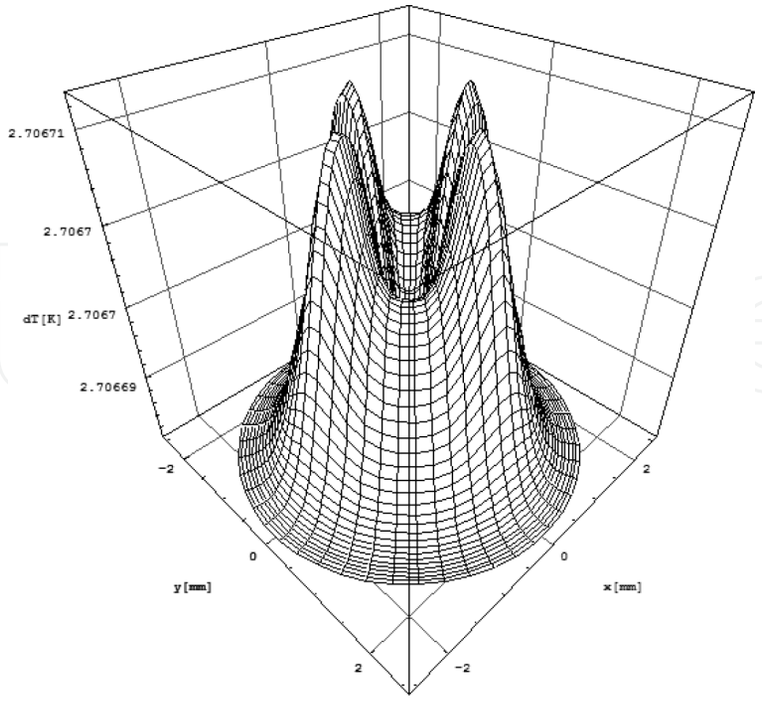

Figure 3. The thermal field produced by four nano-particles-clusters on a Cu substrate. The depth is also 200 nm.

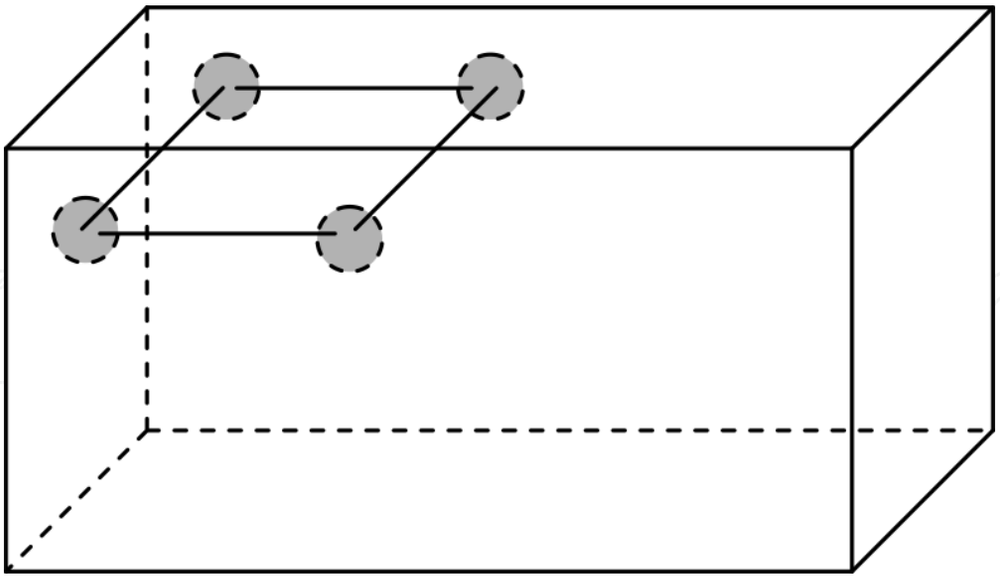

Figure 4. The "geometrical" situation for **Figure 3**.

3. The applicability of the Fourier heat equation for study of relativistic electron-solid interaction

Taking into account the experimental data that were measured at the ALIN-10 linear accelerator from NILPRP [13] can be approximated a power distribution in the electron beam cross section as follows:

$$\mathbf{P}(\ \mathbf{x},\mathbf{y}) \cong \boldsymbol{P}_0 \cdot \boldsymbol{e}^{-(x^2+y^2/169)}. \tag{6}$$

Therefore, it is supposing that the irradiation source emits relativistic electrons with an asymmetric Gaussian distribution [14, 15]. This intensity distribution of the accelerated electron beam is represented in **Figure 5** and is obtained using the experimental data shown in **Figure 6**. The approximation of the ratio between the two planar coordinates of the electron beam spot is obtained from **Figure 6**. This shows the experimental transverse profile of the beam at the exit of the ALIN-10 accelerator. The average beam power is 62 W for a beam current of 10 μA. The measured beam dimensions in the transverse plane are 14 and 2 mm on the x and y coordinates.

The normalization condition is:

$$\int_{-2}^{2}\int_{-8}^{8} e^{-(x^2+y^2/169)}\boldsymbol{dxdy} = 13\pi \cdot \boldsymbol{Erf}[8/13] \cdot \boldsymbol{Erf}[2] \cong 25.3 \tag{7}$$

http://dx.doi.org/10.5772/62353

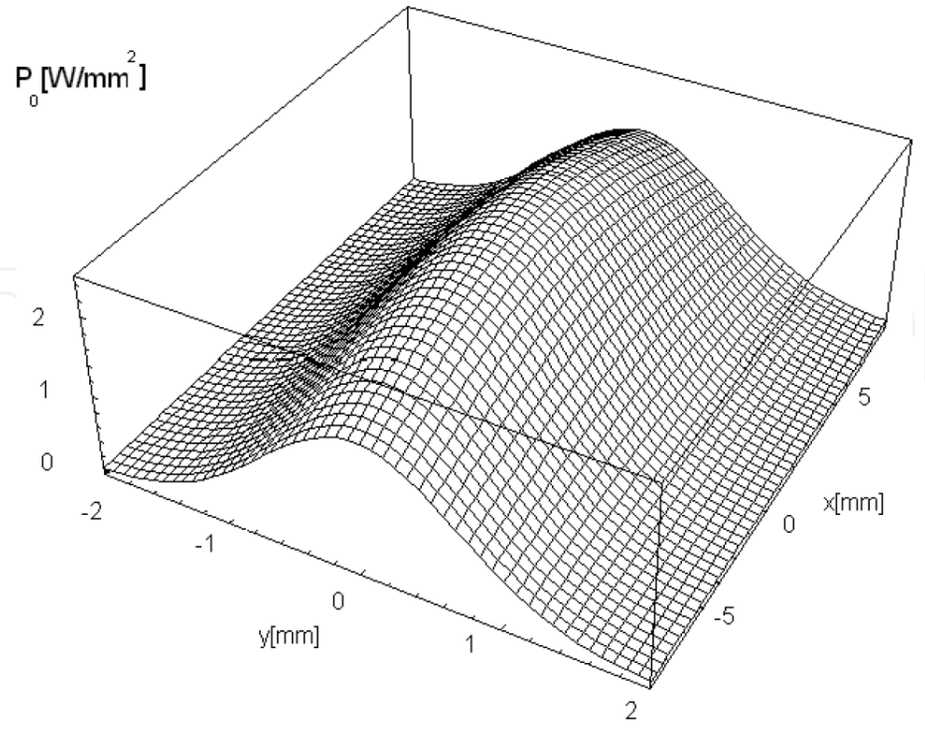

Figure 5. The simulated intensity in the cross section of the beam delivered by ALIN-10.

Taking into account that the average power in time of the electron beam is 62 W, we obtain $P_0 = 2.45\ W$.

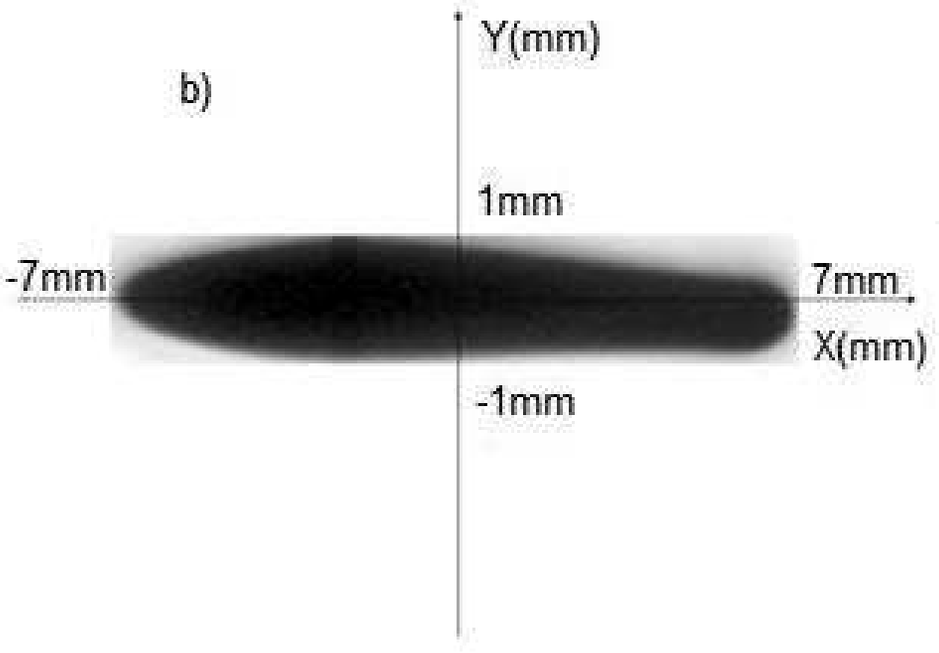

Figure 6. The experimental spot on a plastic sample due to the electron beam after a 10 s exposure.

The geometry of the simulation is shown in **Figure 7** where the electron beam propagates along the z axis and is incident on a graphite sample with dimensions 10 × 10 × 15 mm. The geometry is described in Cartesian coordinates and the transversal plane of the beam is the xy plane.

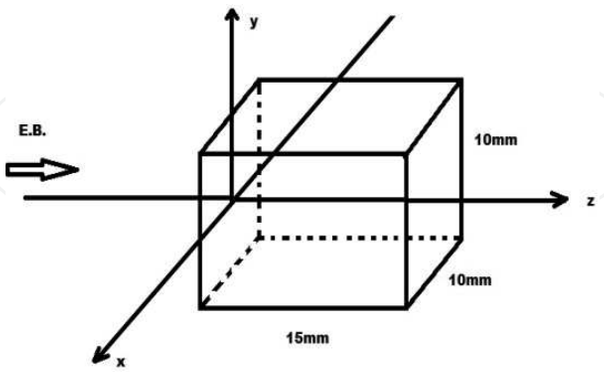

Figure 7. Irradiation geometry for a small graphite sample.

The instantaneous energy loss of electrons passing through the material sample ($\propto \partial E/\partial z = f(E, M_i)$) depends on material constants such as the mass density of the target, the atomic number, the classical radius of the electron and some empirical numerical constants, and does not depend explicitly on the distance travelled, in our case the z direction. When calculating the stopping power, three physical phenomena are taken into account: the secondary electron emission, the polarization of the target and the effect of magnetic field on the incident beam [16, 17].

For electrons with energies greater than 2.5 MeV, their range in the target material is given by the formula put forward by Katz and Penfolds [18]:

$$\boldsymbol{d}_{\max}[\boldsymbol{cm}] = (0.530 \cdot \boldsymbol{E}_{\max}[\boldsymbol{MeV}] - 0.106[\boldsymbol{cm}]) / \rho[\boldsymbol{g} / \boldsymbol{cm}^3]. \tag{8}$$

Here, $d_{\max}$ represents the maximum range of electron beam given in cm in a target of density ρ expressed in g/cm^3. The energy E_{max} is introduced in expression of Eq. (8) in MeV and it refers to the maximum energy of the beam which determines the maximum range that the electrons of the beam can go through in a target. Based on this equation, a linear dependency of the energy absorbed in the material with the distance z is considered.

In our study it has used a graphite sample with ρ = 2.23 g/cm^3 giving d_{max} = 1.43 cm, below the length of our sample. This leads to the following absorption law:

$$\boldsymbol{E}_{abs}(\boldsymbol{z}) = \begin{cases} 6.23 - 4.36 \cdot \boldsymbol{z}, \boldsymbol{for}\, \boldsymbol{z} \le \boldsymbol{d}_{\max} \\ 0, \boldsymbol{for}\, \boldsymbol{z} > \boldsymbol{d}_{\max} \end{cases}, \tag{9}$$

http://dx.doi.org/10.5772/62353

where: E_{abs} is in MeV and z is expressed in centimeters. Expression of Eq. (9) is the source term for the heat equation as it will be shown in the next section.

4. The Fourier heat equation

The goal to establish the thermal field during electron beam irradiation is not a new issue. For achieving it in the irradiation geometry described in **Figure 7**, the heat equation in Cartesian coordinates is the starting point:

$$\frac{\partial^2 \boldsymbol{T}}{\partial \boldsymbol{X}^2} + \frac{\partial^2 \boldsymbol{T}}{\partial \boldsymbol{Y}^2} + \frac{\partial^2 \boldsymbol{T}}{\partial \boldsymbol{Z}^2} - \frac{1}{\gamma}\frac{\partial \boldsymbol{T}}{\partial \boldsymbol{t}} = -\frac{A(\boldsymbol{X},\boldsymbol{Y},\boldsymbol{Z},\boldsymbol{T})}{\mathbf{k}} \tag{10}$$

Here T represents the temperature variation relative to the initial sample temperature T_0, which occurs during exposure to the electron beam, A is the energy deposited by electrons in the unit volume and unit time, k is the thermal conductivity and γ is the thermal diffusivity of the sample. We have $A(x, y, z, t) = E_{abs}(z)/(V_{sample} \times t_0)$, where $V_{sample} = a \cdot b \cdot c$ and t_0 is the irradiation time. The boundary conditions are:

$$\left[\frac{\partial K_x}{\partial X} + \frac{h}{k}\cdot K_x\right]_{x=-\frac{a}{2}} = 0, \quad \left[\frac{\partial K_x}{\partial X} + \frac{h}{k}\cdot K_x\right]_{x=\frac{a}{2}} = 0, \tag{11a}$$

$$\left[\frac{\partial K_y}{\partial Y} + \frac{h}{k}\cdot K_y\right]_{y=\frac{b}{2}} = 0, \quad \left[\frac{\partial K_y}{\partial Y} + \frac{h}{k}\cdot K_y\right]_{y=-\frac{b}{2}} = 0, \tag{11b}$$

$$\left[\frac{\partial K_z}{\partial Z} - \frac{h}{k}\cdot K_z\right]_{z=0} = 0, \quad \left[\frac{\partial K_z}{\partial Z} + \frac{h}{k}\cdot K_z\right]_{z=c} = 0, \tag{11c}$$

where a, b and c are the geometrical lengths of the sample, along X, Y and Z, respectively, h is the heat transfer coefficient, K_x, K_y, K_z are the Eigen functions and α_i, β_j,χ_o are their corresponding Eigen values, respectively.

The solution for the heat equation is:

$$\Delta T(x,y,z,t) = \sum_{i=1}^{\infty}\sum_{j=1}^{\infty}\sum_{o=1}^{\infty} I_1(\alpha_i,\beta_j,\chi_o) I_2(\alpha_i,\beta_j,\chi_o,t) K_x(\alpha_i,x) K_y(\beta_j,y) K_z(\chi_o,z), \tag{12}$$

where

$$I_1(\alpha_i,\beta_j,\chi_o)=\frac{1}{C_iC_jC_o}\int_{-\frac{a}{2}}^{\frac{a}{2}}\int_{-\frac{b}{2}}^{\frac{b}{2}}K(\alpha_i,x)K(\beta_j,y)\cdot P(x,y)\cdot dxdy\int_0^c K_o(\chi_o,z)(6.23-4.36\cdot z)dz,$$
$$I_2(\alpha_i,\beta_j,\chi_o,t)=\frac{1}{\alpha_i^2+\beta_j^2+\chi_o^2}[1-e^{-\gamma_{ijo}^2 t}-(1-e^{-\gamma_{ijo}^2(t-t_o)})h(t-t_o)], \quad (13)$$

with

$$\gamma_{ijo}^2=\gamma(\alpha_i^2+\beta_j^2+\chi_o^2) \quad (14)$$

Here, C_i, C_j, C_o are normalization constants. The Eigen functions determined for the heat equation (10) with boundary conditions (11a–c) have the following explicit expressions:

$$K_x(\alpha_i,x)=\cos(\alpha_i\cdot x)+(h/k\alpha_i)\cdot\sin(\alpha_i\cdot x) \quad (15a)$$

$$K_y(\beta_j,y)=\cos\left(\beta_j\cdot y\right)+(h/k\beta_j)\sin\left(\beta_j\cdot y\right) \quad (15b)$$

$$K_z(\chi_0,z)=\cos\left(\chi_0\cdot z\right)+(h/k\chi_0)\sin\left(\chi_0\cdot z\right) \quad (15c)$$

The Eigen values can be determined from the boundary equations:

$$2\cot\left(\alpha_i a\right)=\frac{\alpha_i k}{h}-\frac{h}{k\ \alpha_i} \quad (16a)$$

$$2\cot\left(\beta_j b\right)=\frac{\beta_j k}{h}-\frac{h}{k\beta_j}, \quad (16b)$$

$$2\cot\left(\chi_0 c\right)=\frac{\chi_0 k}{h}-\frac{h}{k\ \chi_0}. \quad (16c)$$

5. Experiment and simulations

For small samples the thermal field distribution is determined by two important factors: the energy denoted by the term A in Eq. (10) released by the electrons during the time and volume

http://dx.doi.org/10.5772/62353

unit within the target, and the heat transfer constant *h*, which shows how fast the target loses its heat to the surrounding environment depending on the material of the target, pressure of the surrounding gas and magnitude of the contact surface between the target and the environment. The temperature increases with the absorbed energy *A*, and with the decrease of *h.* There are in general three types of heat transfer by: (i) radiation, (ii) convection and (iii) conduction. In the present case, the heat lost by conduction is neglected as the sample is fixed on two Teflon claws. The heat rate lost by radiation may be written as $\sigma \cdot E \cdot \left(T^4 - T_0^4\right)$, which in linear approximation is given by $4\sigma \cdot T_0^3 \cdot E \cdot (T - T_0) \equiv h_{rad} \cdot (T - T_0)$. Here, $h_{rad} = 4 \cdot \sigma \cdot T_0^3 \cdot E$, where $T_0 = 298$ K, $\sigma = 5.6 \times 10^{-8}$ $Wm^{-2}K^{-4}$ is the Stephan Boltzmann constant, and *E* is the thermal emissivity which for polished metallic surfaces can be taken as 0.05. We obtain $h_{rad} = 3 \cdot 10^{-7} W mm^{-2} K^{-1}$. The heat rate loss by convection when the sample is in air obeys a power law given by: $20 \cdot 10^{-9} (T - T_0)^{5/4} [W mm^{-2}]$. This expression can be further made linear: $20 \cdot 10^{-9} (T - T_0)^{1/4} (T - T_0) [W mm^{-2}] = h_{conv} \cdot (T - T_0) [W mm^{-2}]$. In consequence we can conclude: $h_{conv} \cong 0.8 \cdot 10^{-7} W mm^{-2} K^{-1}$, where we have considered: $T - T_0 = 300K$. The total heat transfer coefficient is: $h_{total} = h_{rad} + h_{conv} \cong 3.8 \cdot 10^{-7} W mm^{-2} K^{-1}$, which corresponds to the sample surrounded by air. For a sample in vacuum we neglect cooling by convection $h_{conv} = 0$, and therefore: $h_{total} = h_{rad} \cong 3 \cdot 10^{-7} W mm^{-2} K^{-1}$.

The temperature of a rectangular graphite sample was measured using two thermocouples attached on the lateral and back sides of the sample, respectively. No thermocouple was mounted on the face directly exposed to the incident electron beam to prevent the obstruction of the beam and to protect the sensor. The beam was incident on the square face of the sample with a cross section of 10 × 10 mm and propagated along its length of 15 mm. Each thermocouple consisted in a small size junction with a rounded head of about 1 mm in diameter and was connected to a FLUKA unit which displayed in real time the measured temperature during irradiation. The acquisition of temperature time series was done simultaneously with the two thermocouples. The electron beam exited the vacuum structure of a low-power LINAC through an aluminum window and was incident on the sample placed in air, at normal pressure and temperature. The irradiation time was limited to a few tens of seconds such that no damages would be induced in the sample, its support and the thermocouples. Longer irradiation times of over 50 s could easily induce temperatures well above 500°C.

Figures 8 and **9** present the evolution in time of the temperature on the surface of the graphite sample at two locations (x, y, z) given by (5, 0, 7.5 mm) and (0, 0,15 mm), respectively. Both locations were conveniently chosen to be at the center of the sample faces and coincided with the position of the sensors. In the figures T_{sample} is the temperature of the sample in Celsius. The irradiation time was 36 s, during which T_{sample} increased continuously. When the irradiation stopped, the temperature started to decrease and the sample cooled down. One can observe that T_{sample} dropped relatively fast during the first 20 to 30 s of cooling down process and at a much slower rate after about 100 s.

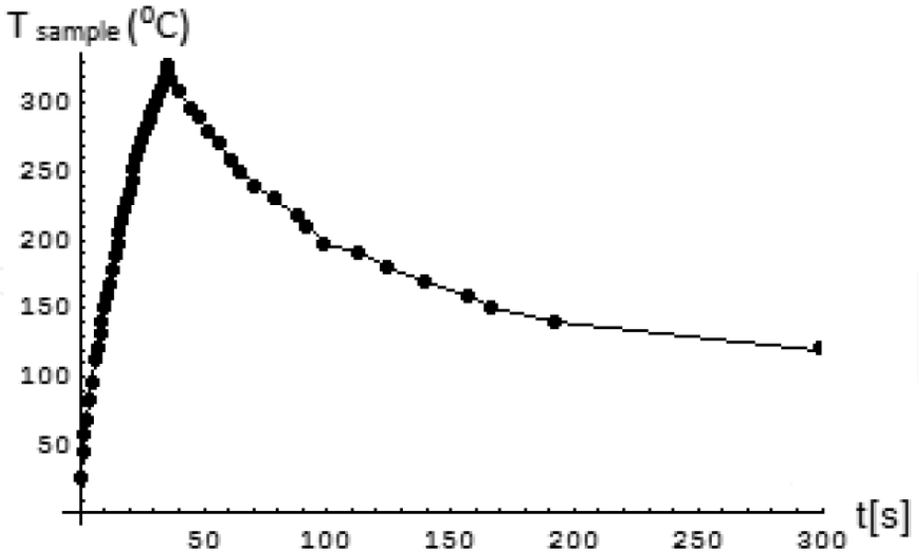

Figure 8. The experimental results for temperature variation in time at the point (x, y, z) = (5, 0, 7.5 mm).

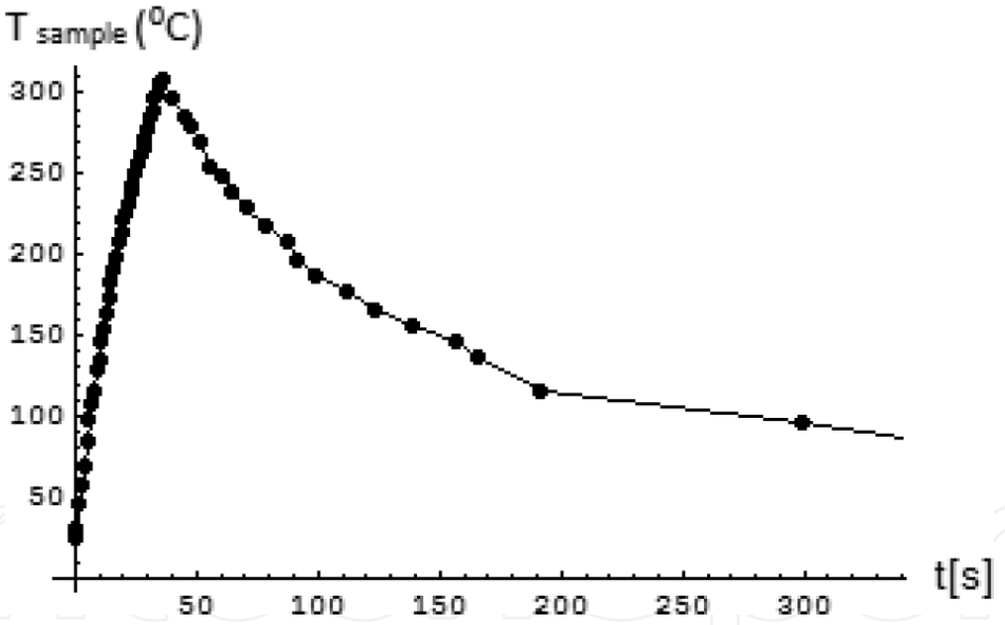

Figure 9. The experimental results for temperature variation in time at the point (x, y, z) = (0, 0, 15 mm).

In **Figure 8** a slightly higher peak in the temperature with about 30 degrees is observed compared to **Figure 9**. The reason is that the position on the sample surface at which data presented in **Figure 8** has been recorded was closer to the heating source. **Figures 10** and **11** present the comparison of experimental data (dotted line) with our simulations (continuous line) according to integral transform technique. The agreement is quite well, an improving of the future simulations being the consideration of non-Fourier models.

http://dx.doi.org/10.5772/62353

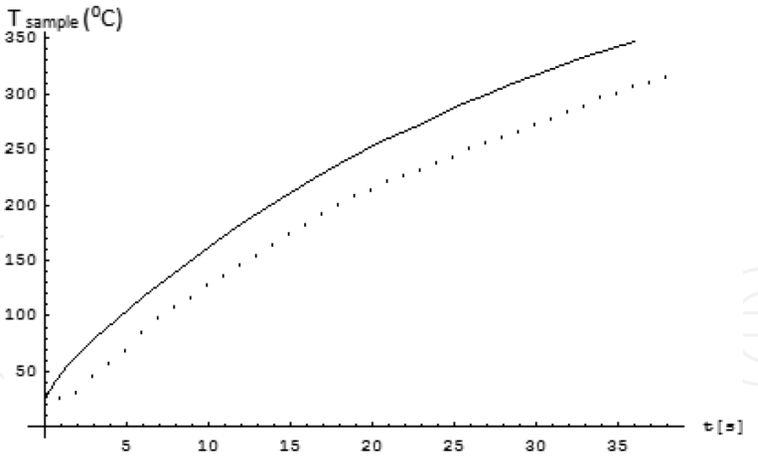

Figure 10. The experimental (dotted line) and simulation (continuous line) results for temperature versus time at the point: (x, y, z) = (5, 0, 7.5 mm), during 36 s irradiation time.

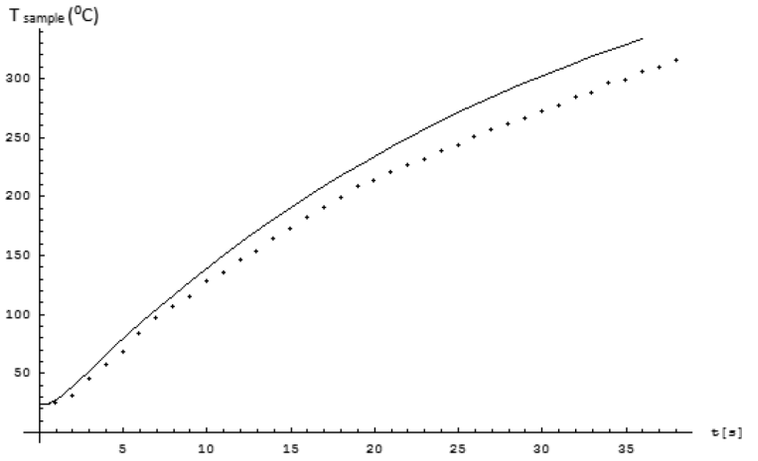

Figure 11. The experimental (dotted line) and simulation (continuous line) results for temperature versus time at the point: (x, y, z) = (0, 0, 15 mm), during 36 s irradiation time.

6. Laser versus electron interaction in w bulk target processing

As it is known, in the case of a Gaussian laser beam having a waist of w = 1 mm, the Lambert Beer absorption law reads:

$$I_{mn}(x,y) = I_{0mn}(x,y) \times Exp[-\alpha z] \tag{17}$$

$$I_{mn}(x,y) = I_{0mn}\left[H_m(\tfrac{\sqrt{2}x}{w})H_n(\tfrac{\sqrt{2}y}{w}) \times Exp\left[-\left(\tfrac{x^2+y^2}{w^2}\right)\right]\right]^2 \tag{18}$$

Here, I_{mn}, I_{0mn}, H_m, H_n are lasers intensity in the mode {*m*,*n*}, maximum laser intensity in the mode {*m*,*n*}, the Hermite polynomial of order *m*, respectively of order *n*. We are dealing with CO_2 lasers in *cw* mode.

We assumed that one is in the case: $m = 0$ and $n = 0$ in Eq. (18).

For electron irradiation, one should apply, in the particular case of *W*, the empirical absorption Tabata-Ito-Okabe law [19]; it is also considered a Gaussian profile of the electron beam.

The total power of the laser and electron beams is around of 200 W.

The maximum propagation length of an electron beam in cm in targets with high *Z* of density ρ expressed in g/cm^3 is:

$$d_{\max} = a_1 \left[\left(1/a_2\right) \ln \left(1 + a_2\tau\right) - a_3\tau \ / \left(1 + a_4\tau^{a5}\right) \right] / \rho \tag{19}$$

Here, τ is a unitless ratio between the kinetic energy of the electron beam (express in MeV) and the electron rest mass energy.

$$a_1 = b_1 A / Z^{b2},\ a_2 = b_3 Z,\ a_3 = b_4 - b_5 Z,\ a_4 = b_6 - b_7 Z,\ a_5 = b_8 / Z^{b9} \tag{20}$$

The constants b_i are given in Table 2:

i	b_i
1.	0.2335
2.	1.209
3.	1.78×10^{-4}
4.	0.9891
5.	3.01×10^{-4}
6.	1.468
7.	1.180×10^{-2}
8.	1.232
9.	0.109

Table 2. The constants b_i in Tabata-Ito-Okabe formula.

Following the formalism from our previous paper, one may write:

$$E_{abs}(z) = \begin{cases} 6.23 - 49.84 \cdot z, for\, z \le 0.125\ cm \\ 0, for\, z > 0.125\ cm \end{cases} \tag{21}$$

http://dx.doi.org/10.5772/62353

where z, E are expressed in cm and MeV, respectively.

In **Figures 12** and **13**, we present the variation of thermal fields under laser and electron irradiation at the same continuous power (200 W) after an exposure time of 25 s. It can be observed that the thermal fields are almost identical, despite the fact that Lambert Beer law (Eq. (17) with: ($\alpha = 8 \times 10^{-2}\text{cm}^{-1}$)) and Tabata-Ito-Okabe (Eq. (21)) law are quite different.

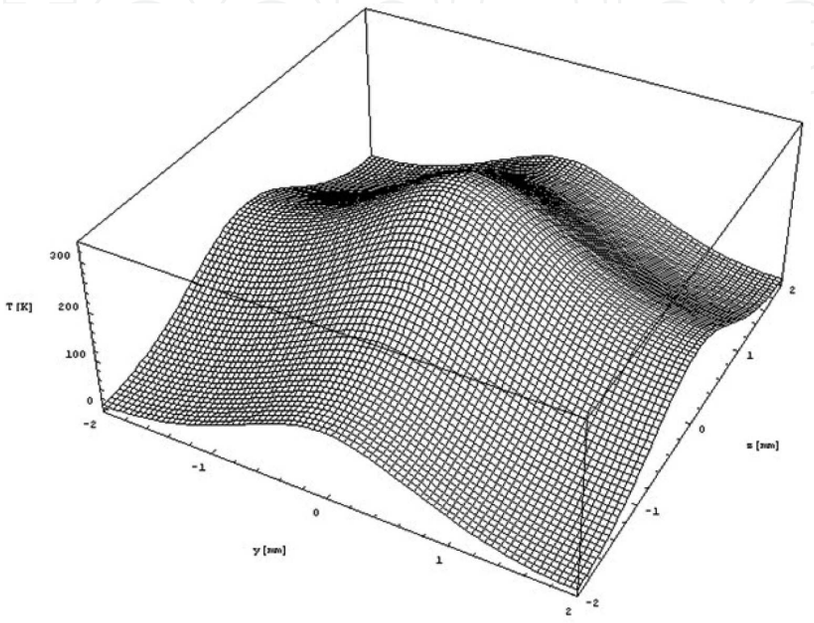

Figure 12. Temperature field on W surface after 25 s irradiation with an IR laser beam of 200 W power. In the integral transform technique T is the variation temperature rather than the absolute temperature.

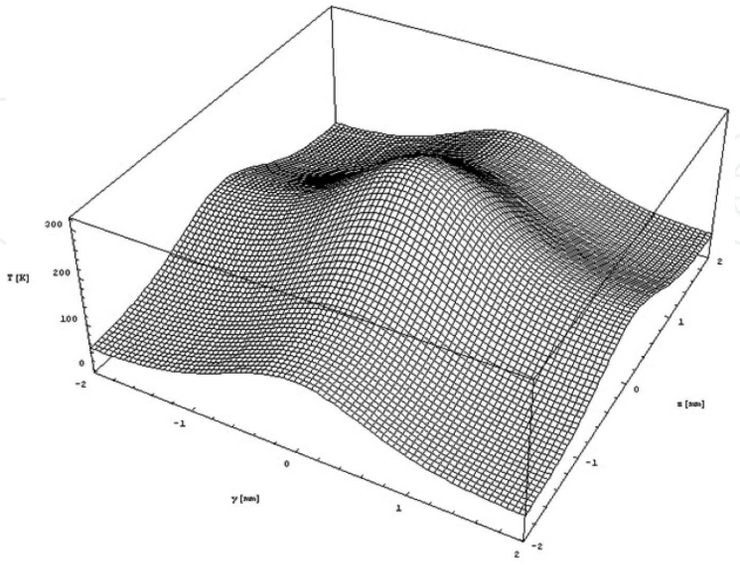

Figure 13. Temperature field on W surface after 25 s electron beam irradiation at 200 W power and 6.5 MeV energy.

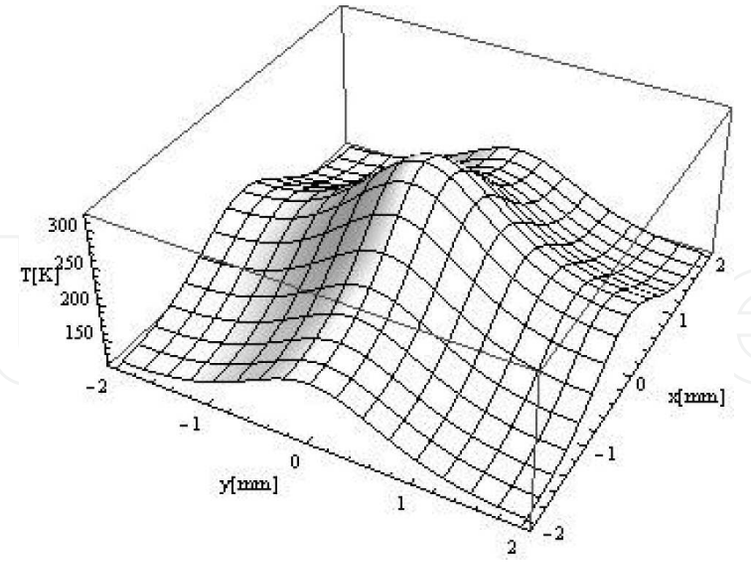

Figure 14. Temperature field on graphite surface after 20 s irradiation with an IR laser beam of 250 W power. In the integral transform technique T is the variation temperature rather than the absolute temperature.

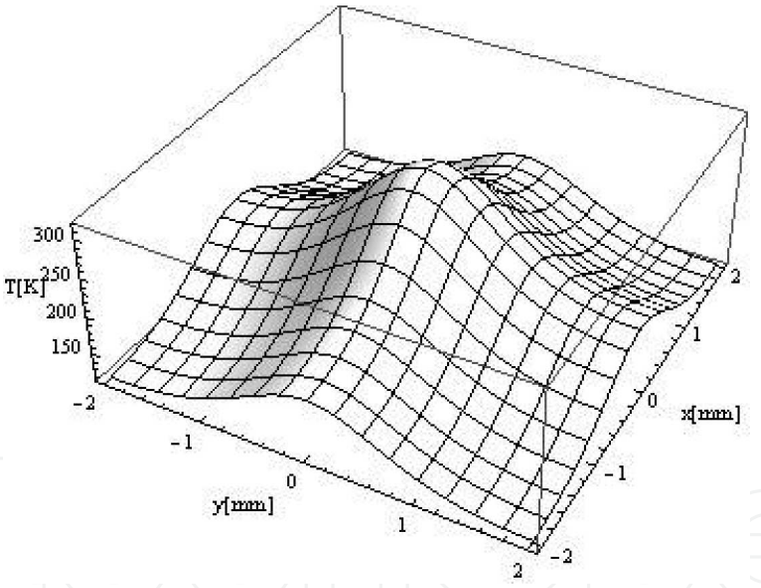

Figure 15. Temperature field on graphite surface after 20 s electron beam irradiation at 250 W power and 6.5 MeV energy.

In **Figures 14** and **15** we present the variation of the thermal fields under laser and electron irradiation at the same continuous power (250 W) after an exposure time of 20 s. Noticeably, the thermal fields are almost identical, also despite the fact that Lambert Beer law ($\alpha = 10^{-1}\text{cm}^{-1}$) and Katz and Penfolds (Eq. (9)) law are quite different. This implies that initial supposition regarding the similarity between laser and electron irradiation at relatively high power is fully justified. For the near future shall be developed non-Fourier models in order to be more accurate in the tentative to explain the experimental data [20, 21].

http://dx.doi.org/10.5772/62353

Acknowledgements

This work was supported by the NUCLEU project (M. Oane) and M-ERA-NET MAGPHOGLAS/2013-2015—(R.V. Medianu).

Author details

Mihai Oane[1], Rareş Victor Medianu[2*] and Anca Bucă[1]

*Address all correspondence to: vrmlaser@gmail.com or rares.medianu@nanofizica.ro

1 National Institute for Laser, Plasma Radiation Physics, Bucharest, Romania

2 University of Bucharest, Faculty of Physics, Bucharest, Romania

References

[1] Oane M., Ticoş D., Ticoş C. M., Charged Particle Beams Processing Versus Laser Processing (Monograph), Scholars' Press, Germany, 2015; ISBN: 978-3-639-66753-0.

[2] Oane M., Peled A., Medianu R. V., Notes on Laser Processing (Monograph), Lambert Academic Publishing, Germany, 2013; ISBN: 978-3-659-487-48739-2.

[3] Visan T., Sporea D., Dumitru G., Infrared Physics & Technology, 1998, 39, 335–346.

[4] Bozóki Z. , Miklós A., Bicanic D., Applied Physics Letters, 1994, 64, (11), 1362.

[5] Koshlyakov N. S., Smirnov M. M., Gliner E. B., Differential Equations of Mathematical Physics, North-Holland Publishing Company, Amsterdam, 1964.

[6] Cline H. E., Anthony T. R., Journal of Applied Physics, 1977, 48(9), 3895–3900.

[7] Yamada M., Nambu K., Yamamoto K., Journal of Applied Physics, 1985, 57(3), 965–968.

[8] Slusher R. E., Reviews of Modern Physics, 1999, 71(2), 471–479.

[9] Carslaw H. S., Jaeger J. C., Conduction of Heat in Solids, Second edition, Oxford University Press, London, 1959.

[10] Korner C., Bergmann H. W., Applied Physics A, 1998, 67,(67),397-401.

[11] Joseph D. D., Preziosi L., Reviews of Modern Physics, 1989, 61(1),41–73.

[12] Bauerle D., Laser Processing and Chemistry, Springer-Verlag, 1996.

[13] Martin D., Fiti M., Radu A., Dragusin M., Cojocaru G., Margarirescu A., Indreas I., Radiation Physics and Chemistry, 1995, 45(4), 615–621.

[14] Oane M., Toader D., Iacob N., Ticoş C. M., Nuclear Instruments and Methods in Physics Research B, 2014, 337, 17–20.

[15] Oane M., Toader D., IacobN., Ticoş C. M., Nuclear Instruments and Methods in Physics Research B, 2014, 318, 232–236.

[16] Yuan X. H., Robinson A. P. L., Quinn M. N., Caroll D. C., Borghesi M., Clarke R. J., Evans R. G., Fuchs J., Gallegos P., Lancia L., Neely D., Quinn K., Romagnani L., Sam G., Wilson P. A., Mc Kenna P., New Journal of Physics, 2010, 12, 063018.

[17] Mahdav M., Ghazizadeh S. F., Journal of Applied Sciences, 2012, 12(2), 145–152.

[18] Katz L., Penfold A. S., Review of Modern Physics, 1952, 24 (1), 28–44.

[19] Tabata T., Ito R., Okabe S., Nuclear Instruments and Methods, 1972, 103, 85–91.

[20] Wang M., Yang N., Guo Z.Y., Journal of Applied Physics, 2011, 110, 064310.

[21] Oane M., Mihăilescu I.N., Ticoş C. M., Banu N., Mitu L. M., Neguţ I., Mihăilescu N., Ticoş D., Journal of Intense Pulsed Laser and Applications in Advanced Physics, 2015, 5(1), 5–8.